

Rheology and fine-line screen printing of solar cell front-side metallization pastes – What really matters

Max Ailinger^{*}, Karim Abdel Aal, Norbert Willenbacher

Karlsruhe Institute of Technology, Institute of Mechanical Process Engineering and Mechanics, 76131, Karlsruhe, Germany

ARTICLE INFO

Keywords:

Screen printing
Silicon solar cell
Front side metallization
Paste rheology

ABSTRACT

Current solar research focuses on reducing silver consumption in order to enable the large-scale increase in PV installations needed to address climate change and the growing global energy demand. This study explores how rheological properties of metallization pastes, such as yield stress, high shear viscosity, slip stress, and slip velocity, affect fine-line screen printing outcomes, including line width, height, uniformity, and interruptions. A model system based on capillary suspensions using Texanol as bulk liquid and employing four secondary liquids with varying interfacial tension was developed for systematic paste property variations. The resulting capillary suspensions exhibited a yield stress and pronounced wall slip below the yield stress, with the slip layer consisting of the bulk liquid. Particle volume fraction, secondary liquid to particle ratio, and type of secondary liquid were varied to systematically modify yield stress, high shear viscosity, and slip velocity of the pastes. Printing experiments revealed that higher yield stress reduced spreading but maintained similar paste laydown. High shear viscosity was identified as critical for controlling paste transfer and achieving narrow line widths. Excessive slip caused inhomogeneous line morphology and reduced paste transfer, indicating an optimal slip range for high-quality printing. These findings were applied to develop a metallization paste achieving a 24 μm line width and 0.48 aspect ratio, achieving an efficiency of 23.53 % for PERC cells with 16 % lower laydown than commercial pastes. This study highlights the importance of yield stress, viscosity, and slip in screen printing, aiding future paste development to reduce silver consumption in photovoltaics.

1. Introduction

The crystalline silicon solar cell production in 2024 was around 560 GWp [1] with forecasts indicating an increase to 4500 GWp by 2050 [2]. This rapid growth raises concerns regarding the raw material supply, particularly the availability of silver, since the photovoltaic industry already consumed 19 % of the global silver supply in 2024 [3]. Consequently, and also given that silver accounts for 10–20 % of the total cell production cost [4,5], current research is exploring alternative metallization materials, like copper and aluminum. However, these metals show higher bulk resistivity ($\rho_{\text{Cu}} = 1.6 \times 10^{-8} \Omega\text{m}$ and $\rho_{\text{Al}} = 2.5 \times 10^{-8} \Omega\text{m}$) compared to silver ($\rho_{\text{Ag}} = 1.5 \times 10^{-8} \Omega\text{m}$) [6]. Furthermore, copper and aluminum may deteriorate cell efficiency due to undesirable interactions with the crystalline silicon [7,8]. Due to persistent challenges, which also include long-term stability, this technological approach is still on the research and development level and almost all industrial cell production lines still employ silver pastes for frontside metallization.

The current solution to reduce the silver consumption is to decrease

the finger cross sectional area. For this reason, progressively thinner fingers are applied to the front side of solar cells using the screen-printing process [2]. An additional benefit of reduced line width is a reduction in shading, which in turn increases cell efficiency. Both effects lead to an increase in rated power per mg of silver used. The reduction in silver consumption is limited by the increasing finger resistance and resulting resistive losses with decreasing cross-sectional area. To counteract this, the line height can be increased [5,9–11].

Commercially available silver pastes contain a high mass fraction of silver particles around 90 wt% (about 48 vol%) and a small fraction of glass frit particles required to open the passivation layer. The particles are dispersed in an organic vehicle consisting of solvents, binders and non-volatile polymeric rheology modifiers, including thixotropic agents [12–15]. Alternatively, the concept of capillary suspensions can be used to enable pastes without non-volatile additives whose residual carbon may deteriorate conductivity in the sintered lines [16]. The paste composition determines the rheological properties of the metallization paste, such as viscosity, yield stress and wall slip, which together with

^{*} Corresponding author.

E-mail address: max.ailinger@partner.kit.edu (M. Ailinger).

the printing technology and the parameters of the specific setup, influences the resulting line morphology. In addition, commercial metallization pastes also typically exhibit viscoelastic properties [17–19]. Thixotropic agents generally infer long relaxation times and a high elastic modulus, while binders contribute weak viscoelasticity and a distribution of shorter relaxation times [20]. However, this study focuses on how yield stress, slip and high shear viscosity affect the screen-printing behavior of model pastes, and in order to avoid contributions due to viscoelastic phenomena we designed a polymer-free paste system. Pastes for screen printing commonly show a shear thinning behavior, i.e. a decrease in viscosity with increasing shear rate, respectively shear stress [17,21–23]. The pastes also exhibit a yield stress σ_y , which denotes the sharp transition from solid-like to liquid-like behavior as the shear stress is increased [22–24]. At stresses below the yield stress σ_y no shear flow occurs but the sample deforms elastically. However, movement of the paste relative to the surfaces it is in contact with may occur at stresses below the yield stress σ_y , this phenomenon is usually termed wall slip. It must be distinguished between true wall slip when the fluid loses its adhesion to the wall and apparent wall slip [25], which is a common phenomenon for highly filled suspensions [26–29] including metallization pastes [30,31]. The rigid particles suspended in the paste cannot penetrate the adjacent wall which leads to a particle depleted layer next to the wall [25]. The thickness of the slip layer is correlated to the size of the particles, and slip layer height over mean particle diameter ratios between 0.04 and 0.09 have been reported [28,32,33]. The viscosity in the slip layer is lower and correspondingly the shear rate is locally much higher than in the bulk fluid due to the decreased particle concentration [29,34]. This is approximately referred to as plug flow, since mass transport is essentially facilitated by the shear flow in the thin slip layer whereas the rest of the fluid is essentially undeformed. It is often assumed that the slip layer essentially consists of the suspensions continuous phase and behaves like a Newtonian fluid [29] and that the slip layer height is directly proportional to the viscosity of the liquid in the slip layer and the slip velocity [28]. It was found that slip sets in at a critical stress σ_s , hereafter termed slip stress, well below the yield stress σ_y of the paste [26,27,31]. In this stress regime, $\sigma_s < \sigma < \sigma_y$, paste flow can be solely attributed to the apparent wall slip. Wall slip may also occur at shear stresses above σ_y . Then shear deformation and plug flow are superimposed [28,35,36].

The screen-printing process is the most widely used industrial process for the metallization of solar cells [2]. During the printing process the paste is excessively sheared when being transferred through a line opening to the substrate. The squeegee that presses the paste through the screen forms a paste roll in front of it. Flow dynamic modeling assuming Newtonian behavior of the paste indicates that this roll acts as hydrodynamic pump which generates the high pressure needed to press the paste through the line openings. This pressure build-up depends on the paste viscosity [37].

Highly filled screen-printing pastes commonly show a shear thinning behavior and exhibit a yield stress and slip properties. Studies on this type of paste have shown that the fine-line screen printing process can be divided into several phases. These are the pre-injection zone, where the paste is pushed through the screen underneath of the paste roll, the cling zone, where the screen clings to the substrate after passage of the squeegee and the snap off, where the screen detaches from the substrate [20]. When the squeegee presses the screen onto the substrate, the paste spreads between the screen and the substrate and subsequently retracts during snap off [20,38]. As confirmed for different types of metallization pastes, spreading and retraction are the key mechanisms in screen printing and the final line width is essentially set when the screen detaches from the substrate [38]. Depending on printing parameters, this happens on a time scale between 10 and 100 ms [38], i.e. much faster than typical flow phenomena, that can be captured using classical rheological measurements, such as the widely used three interval thixotropy tests performed on a rotational rheometer [17]. Nevertheless, an inverse linear relationship between line width and the product of high

shear viscosity and yield stress has been proposed [20].

During snap-off, the paste exhibits shear flow if it experiences shear stresses above the yield stress or slip and, thus, plug flow for shear stresses between slip and yield stress [31]. The latter can be beneficial to reduce line interruptions and increase the aspect ratio [30,31]. Using pastes with slip velocities in the range of 0.25–1.25 mm/s at a shear stress of 300 Pa it could be shown, that a higher slip velocity results in a significantly higher paste transfer and increased line height [30]. This was confirmed by another study employing screens with different surface treatment resulting in different slip [31]. No effect of slip on printing results was found in another study using pastes with about an order of magnitude lower slip velocities [24].

In order to further reduce the silver consumption in frontside metallization of solar cells, a still deeper understanding of the screen-printing process and how paste flow properties affect the printing results is mandatory. In particular, the relevance of the pastes' yield stress and high shear viscosity should be analyzed. Furthermore, it should be investigated whether a strong increase in slip velocity offers further advantages regarding the resulting line morphology. High temperature metallization pastes are complex, multi-component systems and it is difficult to vary rheological parameters independently. The aim of this study is to gain deeper understanding of how paste slip and flow properties determine screen-printing results using a model system that is as simple as possible and offers the possibility to study the effects of different rheological properties on screen printing results independently. Therefore, the capillary suspension concept [39] is used to modify the flow properties of the paste without changing the composition of the bulk liquid and thus without changing the bulk liquid viscosity or wetting properties. Capillary suspensions are ternary systems containing particles, a bulk liquid phase and a small fraction (typically <5 vol%) of a secondary liquid immiscible with the bulk liquid. This immiscibility induces the formation of a strong, sample-spanning particle network, macroscopically showing up in a pronounced yield stress. Capillary suspensions exist either in the pendular state, when the secondary liquid preferentially wets the particles or in the so-called capillary state, when the secondary fluid does not wet the particles. In both cases, the capillary force controlling structure formation is controlled by the interfacial tension between the two included liquids and by the three-phase contact angle of the secondary liquid on the particle surface. Network strength and thus yield stress can be adjusted in a wide range depending not only on fraction, size and shape of the suspended particles but also on the type and fraction of the secondary liquid [39,40].

This concept was already used to formulate highly conductive printable silver pastes without non-volatile polymeric additives, which may disturb the conductivity of the printed structures [16,41]. The particle network in a capillary suspension rapidly breaks down when the yield stress is exceeded, and does not affect the flow behavior at high shear rates typically relevant in coating or printing processes [42]. The viscosity of the suspension is then controlled solely by the viscosity of the bulk liquid and the volume fraction of particles [43]. Thus, for a constant particle volume fraction, the yield stress and slip behavior can be changed by varying the type and/or amount of secondary liquid without changing the viscosity or wetting behavior of the paste. By altering the particle fraction the paste viscosity can be tuned. Although this has an effect on the yield stress, no effect on slip velocity were observed within the parameter range studied here. Consequently, the present study investigates the influence of viscosity and yield stress at constant slip velocity and the influence of the slip velocity at constant viscosity on the printing results. Therefore, printing trials are conducted and the results are discussed in terms of spreading, the occurrence of interruptions, and the final line morphology, i.e. line height and width.

2. Material and methods

2.1. Paste preparation

The particle morphology can significantly influence the rheological properties of suspensions. This has been investigated for three-phase systems similar to the ones present here using a model system [44]. Here the rheological properties yield stress, slip velocity and high shear viscosity are varied in a wide range, while keeping paste composition as simple as possible and focusing on one type of particles, whose morphology is typical for state-of-the-art high-temperature metallization pastes. The particles used are K-7418P silver particle (Metalor Technologies SA, Switzerland) which exhibit a monodisperse particle size distribution with a mean particle size around $1.4 \mu\text{m}$ and a distribution width of $1.0 \mu\text{m}$. Fig. 1 shows two representative SEM images of the K-7418P silver particle.

The bulk liquid consists of Texanol (Sigma-Aldrich, USA) with a viscosity of $13.8 \pm 0.05 \text{ mPa s}$. Four proprietary immiscible hydrophobic liquids SL1 to SL4 are added as secondary liquids to induce formation of a capillary suspension. These fluids differ in their interfacial tension with Texanol and viscosity but otherwise show similar physical behavior.

The sample preparation method is similar as described in Ref. [16]. The three components, the particles, Texanol and one of the four secondary liquids, are mixed five times at 2000 rpm for 30 s with a non-contact planetary centrifugal mixer (SpeedMixer DAC 150.1 FVZ, Hauschild & Co.KG, Hamm, Germany). Samples were allowed to cool between mixing runs. A three-roll mill (80E, EXAKT Advanced Technologies GmbH, Norderstedt, Germany) was employed to facilitate further deagglomeration of silver particles and homogenization of the paste. The samples were milled three times with gap widths that were successively reduced from initial 60 and $20 \mu\text{m}$ to 45 and $15 \mu\text{m}$ and at least to 30 and $10 \mu\text{m}$. The milling process was conducted at a speed of 70 rpm.

2.2. Methods

2.2.1. Yield stress

For the yield stress measurements, a Physica MCR501 Rheometer (Anton Paar GmbH, Graz, Austria) equipped with a vane geometry ST10-4V-8.8 was used. The vane has four blades with 8.8 mm length, and its diameter is 10 mm . The shear stress is set to zero for 3 min with the vane submerged in the sample to exclude any potential stress relaxation effects. Then, the shear stress is increased in 61 logarithmic steps from 1 to 1000 Pa while every step takes 15 s and the deformation is recorded. To determine the yield stress, the deformation is plotted against the shear stress, and a tangent is fitted to the linear-elastic range and the flow region. The intersection of these tangents represents the yield stress [45]. The temperature was set to $25.00 \pm 0.05 \text{ }^\circ\text{C}$.

2.2.2. Wall slip measurement

The wall slip measurement protocol is adapted from Refs. [30,45]. For slip stress and slip velocity measurements below the yield stress the rotational rheometer Haake Mars (Thermo Scientific, Karlsruhe, Germany) equipped with the parallel plate PP20 measuring fixture (radius $R = 10 \text{ mm}$, stainless steel, roughness $R_z = 2.08 \pm 0.34 \mu\text{m}$). A custom-made, bottom plate is used so that the paste is held in place and can only slip on the top plate. The plate-plate distance is set to 2.9 mm . The shear stress is set to zero for 3 min to exclude any potential relaxation effects. The measurement is carried out at 41 stepwise logarithmically increasing shear stress values in the range from 10 to 1000 Pa , each step takes 30 s. The temperature was set to $25.00 \pm 0.05 \text{ }^\circ\text{C}$. The rotation speed n of the top plate is recorded for each stress and the circumferential velocity at the plate rim is taken as slip velocity $v_s = 2\pi Rn$ [30]. Fig. 2 schematically shows the variation of the slip velocity as a function of shear stress. Three regimes are observed: in the first regime slip layer formation takes place and a motion of the upper plate is hardly detectable, then at a critical stress, termed slip stress σ_s , a sharp increase of v_s takes place after which the slip velocity increases almost linearly until the yield stress σ_y is reached. Finally, for $\sigma > \sigma_y$ slip and shear flow are superimposed and for metallization pastes typically sample spillage sets in resulting in a strong increase of apparent slip or upper plate velocity. The slip stress σ_s is determined from the intersection of the tangents fitted to the strongly increasing part of the v_s vs. σ curve at the end of regime I and to the almost linearly increasing part in regime II, the so-called slip regime [30,45,46], as depicted in Fig. 1.

The slip velocity often strongly varies with the applied shear stress, and results for different samples should be compared at a constant shear stress. Here we have chosen a stress value.

$\sigma = 290 \text{ Pa}$, since this value lies in the slip regime of the investigated samples. The apparent slip layer height h_s at the rim of the rheometer plate in regime II can be calculated from the applied stress σ and the measured velocity v_s using [28]:

$$h_s = \frac{v_s \times \eta_{\text{bulk}}}{\sigma} \quad (1)$$

Where η_{bulk} is the viscosity of the liquid in the slip layer and a uniform shear flow in this narrow layer is assumed. It is further assumed that the slip layer mainly consists of the bulk fluid [29] and shows Newtonian behavior for the systems investigated here. The deformation of the paste underneath the slip layer can be neglected, since $\sigma < \sigma_y$.

2.2.3. Capillary rheometry

Since rotational rheometry measurements were constrained due to slip and sample spillage phenomena, viscosity data at high shear rates well above the yield stress were obtained using a custom build capillary rheometer. The piston had a diameter of 8 mm and piston speed was varied between 0.05 mm/s and 10 mm/s . The resulting pressure drop Δp was obtained using two pressure transducers (XTME-100-190M 140 bar, XTM-100-190M 35 bar, Kulite Semiconductor Products, Inc., New

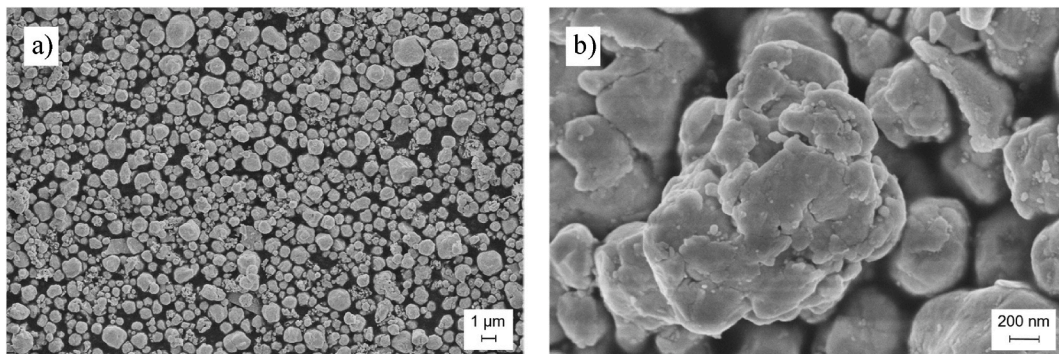


Fig. 1. SEM images of the used K-7418P silver particle with 10.000 (a) and 100.000 (b) magnification.

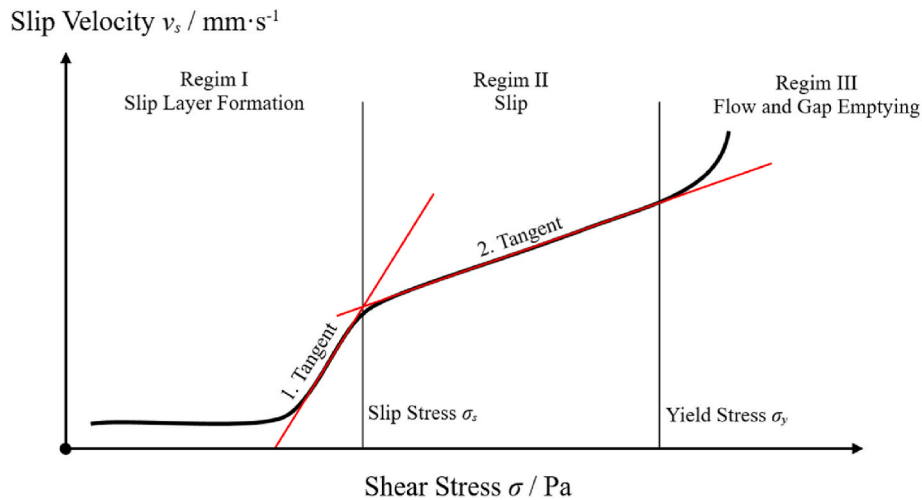


Fig. 2. Schematic representation of the slip velocity v_s as a function of applied shear stress σ . Three regimes are distinguished. Regime I: slip layer formation, regime II: slip regime, regime III: paste flow and gap emptying. The intersection of the tangents fitted to the sharp increase of the v_s - σ curve at the end of regime I (1. Tangent) and the linear branch in regime II (2. Tangent) is used to determine the slip stress as depicted above. The transition between regime II and III is set by the yield stress σ_y .

Jersey, USA) covering the pressure range from 1 to 140 bar. Stainless steel nozzles with different diameter to length ratios were used and the Bagley correction was performed to compensate for the pressure drop contribution due to the inlet and outlet flow effects as described in Refs. [47,48]. Thus, it was possible to cover the shear rate range from 100 s^{-1} to 10.000 s^{-1} and corresponding apparent viscosity data obtained using nozzles with different diameter, but similar diameter to length ratio were evaluated with respect to the relevance of slip phenomena.

2.2.4. Printing setup and evaluation

The printing experiments were conducted on a semi-automatic Ekra E2 screen printing machine (ASYS Automatisierungssysteme GmbH, Dornstadt, Germany). Proprietary, textured, SiN coated high-temperature cell printing dummies were used as substrates. The wafers show the typical pyramid texture with a roughness R_z value of $\approx 6,9 \pm 0,7 \mu\text{m}$. The screens were sourced from Frintrup GmbH (Bonn Beuel, Germany) and utilize a 430–13/17 mesh at an angle of 22.5° with a nominal line opening of $20 \mu\text{m}$. The emulsion over mesh (EOM) layer thickness was $9 \pm 1 \mu\text{m}$. The squeegee used is a diamond squeegee with a hardness of 75 Shore-A. The printing results were compared and evaluated at a printing speed of 300 mm/s , a snap-off distance of 1 mm , and a pressure of 1.5 bar . For the experiments in 3.3 a 480–10/18 knotless screen from Brave C&H Co., Ltd. (Taoyuan City, Taiwan) with similar EOM thickness was used. Printing in 3.3 was done with a 60° and 75 Shore-A squeegee and a printing speed of 500 mm/s , a snap-off distance of 1 mm , and a pressure of 2 bar . The morphology of the wet lines immediately after printing was determined using a laser scanning microscope VK-X100 (Keyence Deutschland GmbH, Neu-Isenburg, Germany) equipped with a Nikon MUL00201 CF Plan 20x objective (20x magnification, numerical aperture $\text{NA} = 0.46$, working distance $\text{WD} = 3.1 \text{ mm}$, Nikon Corporation, Tokyo, Japan). For the evaluation of the line height and optical line width as well as the spreading distance and amount of interruptions the software described in Ref. [38] was used. The code analyzes all 768 pixel lines per image from 3 different randomly distributed pictures from 3 printed substrates per experiment (total of 9 pictures resulting in 6.912 analyzed lines). The line height is defined as the maximum vertical distance of the silver line above the substrate surface, as determined from the height values of the laser scanning image. The optical line width is calculated on the basis of the differentiating grey values between silver and substrate. The maximum spreading distance during printing is indicated by scattered particles in

the pyramid structure of the substrate in the wetted area left and right of the line. The software calculates the mean value and standard deviation of each measured quantity. A pixel line is classified as interruption if no silver deposit is detected based on the grey values. While the printing experiments and line evaluation of the wet lines was done in house, printing and evaluation of the electrical cell properties in 3.3 was done according to standard procedures on a solar simulator at the project partners site as described in Ref. [16].

2.2.5. Interfacial tension measurement

The interfacial tension between the bulk liquid (Texanol) and secondary liquids SL1 to SL4 was measured in accordance with DIN EN ISO 19403-3. A needle with an outer diameter of 1.81 mm was utilized to form a pendant drop of the liquid SL1 to SL4 in Texanol. The drop curvature was subsequently analyzed, and the interfacial tension calculated using the software Drop Shape Analysis (DAS) (KRÜSS GmbH, Germany).

2.2.6. Contact angle measurement

The contact angle was measured based on DIN EN ISO 19403-2. The silver particles were applied to an adhesive tape and a $3 \mu\text{l}$ droplet was placed on the silver particles. The images of the droplets were analyzed using the Drop Shape Analysis (DAS) program (KRÜSS GmbH, Germany) employing the circle fit method.

3. Results and discussion

3.1. Paste rheology

In the following sections, the yield stress as well as slip velocity and slip stress are discussed for three series of model pastes. It is important to note that only one parameter will be varied at once: the particle volume fraction, the secondary liquid to particle ratio, or the interfacial tension between the bulk (Texanol) and the secondary liquid. These model pastes are prepared based on the capillary suspension concept as described above. The contact angle of Texanol on the used silver particles is $26 \pm 2^\circ$, whereas all secondary liquids completely wet the particles. This suggests that the pastes are capillary suspensions in the pendular state [49].

3.1.1. Particle volume fraction

In this section the effect of particle volume fraction on the yield and

slip stress is discussed. Pastes were prepared using Texanol as bulk liquid and SL1 as secondary liquid. Particle volume fraction was varied between 48 and 54 vol%, while the ratio of secondary liquid and particle volume fraction $\phi_{\text{sec}}/\phi_{\text{particle}}$ was held constant at 0.1.

In Fig. 3a and b yield σ_y , and slip stress σ_s are plotted against particle volume fraction ϕ_{particle} . Both quantities increase significantly with increasing ϕ_{particle} . For the yield stress this is consistent with earlier work [40] and reflects the denser network formed with a larger number of particles. The slip stress has not been investigated before for such systems, its increase with increasing particle volume fraction indicates that a higher force is required to form a slip layer, i.e. to displace particles adjacent to the fixture wall.

Fig. 3c shows the slip velocity v_s determined at a shear stress of 290 Pa as a function of particle volume fraction ϕ_{particle} . The slip velocity remains constant at 3.5 ± 0.2 mm/s in the ϕ_{particle} range investigated here. In contrast, earlier work [29] reported a decrease in slip layer and hence slip velocity with increasing particle volume fraction. In this study, however, the particle volume fraction was varied over a wider range for a binary suspension. Here, ϕ_{particle} was varied only in a narrow range, so the geometrical packing constraints close to the wall and hence the slip layer and slip velocity are similar. Nevertheless, the variation in capillary force enabled a substantial variation of slip stress and yield stress.

3.1.2. Secondary liquid fraction variation

In this section the particle volume fraction ϕ_{particle} is held constant at 48 vol%. While the ratio of secondary liquid to particle volume $\phi_{\text{sec}}/\phi_{\text{particle}}$ is varied and again SL1 is used as secondary liquid. Fig. 4a shows the yield stress σ_y as a function of $\phi_{\text{sec}}/\phi_{\text{particle}}$.

The yield stress increases from 50 Pa without secondary liquid to a plateau at 400 Pa when $\phi_{\text{sec}}/\phi_{\text{particle}} = 0.1$ is reached. The increase in yield stress by the factor of eight indicates the formation of a strong particle network controlled by capillary forces [39]. Adding even more secondary liquid results in a saturation of the pendular bridges between particles and the network cannot be reinforced further [49]. The slip stress σ_s (Fig. 4b) displays the same trend as the yield stress, it increases with increasing $\phi_{\text{sec}}/\phi_{\text{particle}}$ until it saturates at $\phi_{\text{sec}}/\phi_{\text{particle}} = 0.1$.

In contrast to slip and yield stress, the slip velocity v_s (Fig. 4c) does not plateau but increases linearly from 2.8 to 5.4 mm/s with increasing $\phi_{\text{sec}}/\phi_{\text{particle}}$. The increase in the slip velocity with constant bulk viscosity η_{bulk} suggests an increase in the slip layer height h_s . A reason for that

could be minor structural changes in the particle network. This aspect will be discussed in more detail in the next section. Irrespective of that, this model system allows us to vary the slip velocity by about a factor of two, while keeping the slip and yield stress, and also the high shear viscosity η_{hs} of the paste constant [42], simply by varying the secondary liquid fraction in the range $\phi_{\text{sec}}/\phi_{\text{particle}} \geq 0.1$.

3.1.3. Variation of the secondary liquid

In this section the influence of the interfacial tension Γ between bulk and secondary liquid is examined using four different secondary liquids SL1 to SL4. The particle volume fraction is kept constant at $\phi_{\text{particle}} = 48$ vol% and the ratio of secondary liquid to particle volume is set as $\phi_{\text{sec}}/\phi_{\text{particle}} = 0.1$. The values for the interfacial tension between Texanol and the liquids SL1 to SL4 as well as the viscosity of these liquids are summarized in Table 1.

In Fig. 5a, the yield stress σ_y is displayed against the interfacial tension Γ between the bulk liquid Texanol and the respective secondary liquid SL1 to SL4. The yield stress apparently increases linearly with increasing interfacial tension, as expected [39], since the surface tension Γ between Texanol and the secondary liquid increases from 0.19 ± 0.01 to 0.51 ± 0.01 mN m⁻¹.

It should be noted, that the viscosity of the secondary liquids SL1 to SL4 varies by about a factor of 47, but previous investigations including different particle types as well as different bulk and secondary liquids clearly revealed that the viscosity of the secondary liquid does not affect the strength of the particle network and hence the yield stress in capillary suspensions [50]. Thus, it has to be assumed that the capillary network and yield stress of the pastes investigated in this study remain unaffected by the different viscosity of the secondary liquids.

In contrast to σ_y , the slip stress σ_s (Fig. 5b) is within experimental uncertainty independent of interfacial tension and values around 170 Pa are found. This is surprising since both yielding of the sample as well as the formation of the slip layer are expected to be related to the network strength. Presumably, the particle network adjacent to the wall exhibits imperfections which facilitate the formation of a slip layer but do not deteriorate the bulk network strength significantly.

Fig. 5c demonstrates that the slip velocity, determined at 290 Pa, increases with increasing interfacial tension. Assuming that the slip layer essentially consists of the bulk fluid, this corresponds to an increase in nominal slip layer height since the bulk viscosity is kept constant. According to Eq. (1) and using the Texanol viscosity ($\eta_{\text{bulk}} = 13.8$

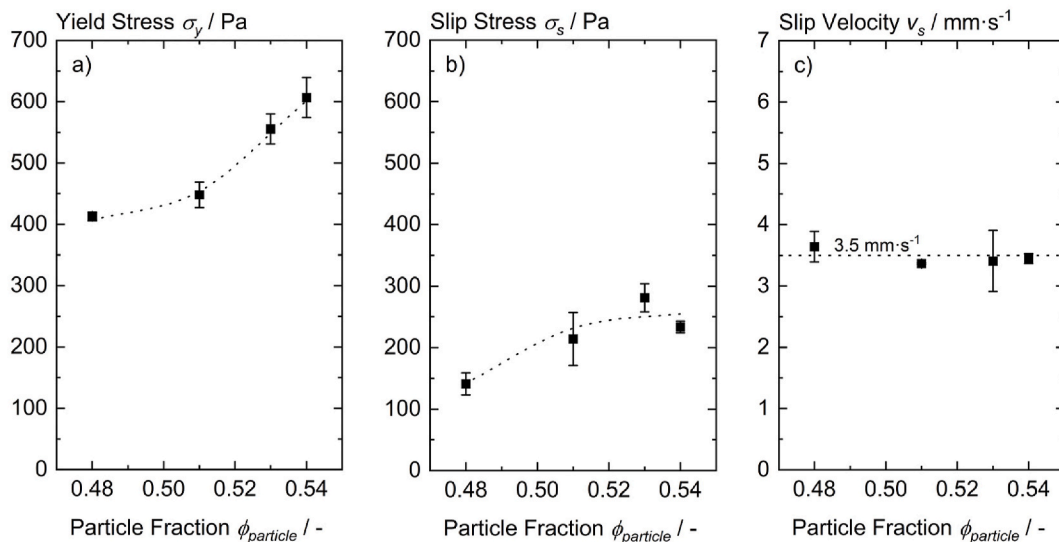


Fig. 3. Yield stress (a), slip stress (b), and slip velocity, determined at 290 Pa, (c) vs. particle volume fraction for pastes including Texanol as bulk phase and SL1 as secondary liquid, ratio of secondary liquid to particle volume $\phi_{\text{sec}}/\phi_{\text{particle}} = 0.1$. The dotted lines are guides for the eye.

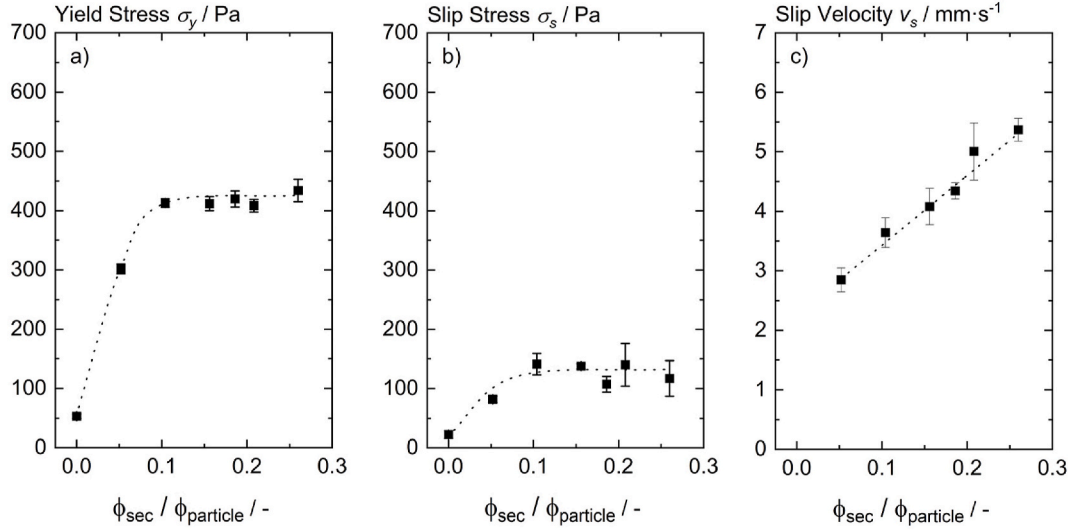


Fig. 4. Yield stress (a), slip stress (b), and slip velocity, determined at 290 Pa, (c) vs. $\phi_{\text{sec}}/\phi_{\text{particle}}$ for pastes including Texanol as bulk phase and SL1 as secondary liquid at a constant particle volume fraction $\phi_{\text{particle}} = 0.48$. The dotted lines are guides for the eye.

Table 1

Interfacial tensions Γ between bulk (Texanol) and secondary liquid as well as the liquid viscosities η .

Liquid	Interfacial tension $\Gamma/\text{mN}\cdot\text{m}^{-1}$	Viscosity $\eta/\text{mPa}\cdot\text{s}$
SL1	0.19 ± 0.01	97 ± 0.02
SL2	0.28 ± 0.01	201 ± 0.6
SL3	0.47 ± 0.01	971 ± 4.6
SL4	0.51 ± 0.01	4605 ± 34
Bulk (Texanol)	–	13.8 ± 0.05

$\pm 0.05 \text{ mPa}\cdot\text{s}$) the slip velocities determined here correspond to slip layer height h_s values between 0.2 and 0.3 μm , i.e. slip layer height to mean particle diameter ratios of 0.1–0.2. This is about twice as high as previously reported for conventional highly filled suspensions above the yield stress [28,32,33], and thus seems to be in a reasonable range.

It is unlikely that the slip layer consists mainly of the secondary

liquid, as this is trapped in the pendular bridges between the particles and is not soluble in the bulk liquid. Moreover, if the slip layer would consist of the secondary liquid, the much higher viscosity of the secondary liquid would correspond to large calculated slip layer heights (Eq. (1)) and consequently lead to high slip layer to particle diameter ratios as shown in Table 2.

The slip layer to particle diameter ratio starts at 0.9 for liquid SL1, which is ten times higher than previously reported ratios of up to 0.09 [28,32,33] and increase to a ratio of 68 for liquid SL4, then exceeding the particle diameter by almost two orders of magnitude which seems to be unphysical. Since, filling this slip layer of approximately 100 μm height would require about one-third of the secondary liquid SL4 to migrate to the wall of the rheometer plate within the short experimental time of about 26 min. Since the pastes remain stable even after being transferred multiple times into different containers and on the three-roll mill, it can be ruled out that significant portion of the secondary phase quantity is lost with each contact with a surface. These considerations further support the assumption, that the slip layer mainly consists of the

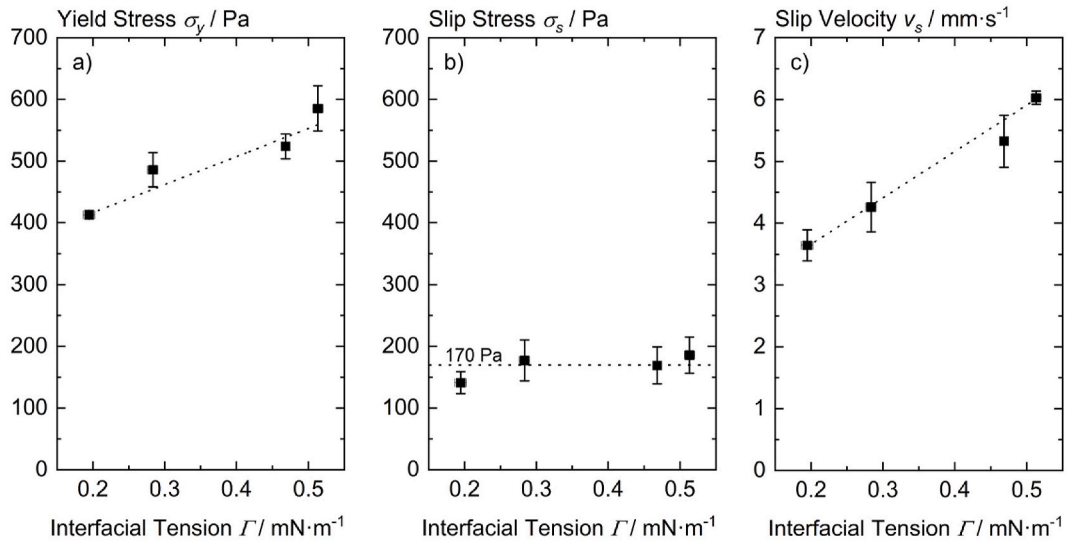


Fig. 5. Yield stress (a), slip stress (b), and slip velocity (c), determined at 290 Pa, vs. interfacial tension between bulk and secondary liquid. The pastes include Texanol as bulk and SL1 to SL4 as secondary liquid with a ratio of secondary liquid to particle fraction $\phi_{\text{sec}}/\phi_{\text{particle}} = 0.1$ and constant particle volume fraction $\phi_{\text{particle}} = 0.48$. The dotted lines are guides for the eye.

Table 2

Calculated slip layer to particle diameter ratio under the assumption that the slip layer consists of the secondary liquid. The slip layer is calculated with Eq. (1), the viscosities in Table 1 and the slip velocity at 290 Pa. The particle diameter is 1.4 μm . The pastes include Texanol as bulk and SL1 to SL4 as secondary liquid with a ratio of secondary liquid to particle fraction $\phi_{\text{sec}}/\phi_{\text{particle}} = 0.1$ and constant particle volume fraction $\phi_{\text{particle}} = 0.48$.

Secondary Liquid	Slip Layer to Particle Diameter Ratio/-
SL1	0.9
SL2	2.1
SL3	12.8
SL4	68.4

bulk liquid.

3.1.4. Slip at high shear rates

Extensive capillary rheometer measurements have been conducted for a paste containing 48 vol% particles (additionally including 2.2 vol% of glass frit) in order to evaluate the relevance of wall slip phenomena under high shear conditions. The paste comprises Texanol as bulk liquid with a ratio of secondary liquid SL1 to particle volume fraction, $\phi_{\text{sec}}/\phi_{\text{particle}} = 0.1$ and particle volume fraction $\phi_{\text{particle}} = 0.48$. Nozzles with different diameter and various diameter to length ratios were used. The latter series allowed for the so-called Bagley correction [47] eliminating inlet and outlet pressure drop contributions to the total measured pressure drop Δp . In Fig. 6 the Bagley corrected apparent viscosity data are plotted as a function of shear rate. As expected the paste exhibits pronounced shear thinning and the viscosity decreases from about 10 to 1 Pa s as the shear rate increases from 100 to 10,000 s^{-1} . The data obtained using nozzles with different diameter, however, do not show a systematic increase of apparent viscosity with increasing diameter, clearly demonstrating that wall slip is not a significant phenomenon at this high shear rates.

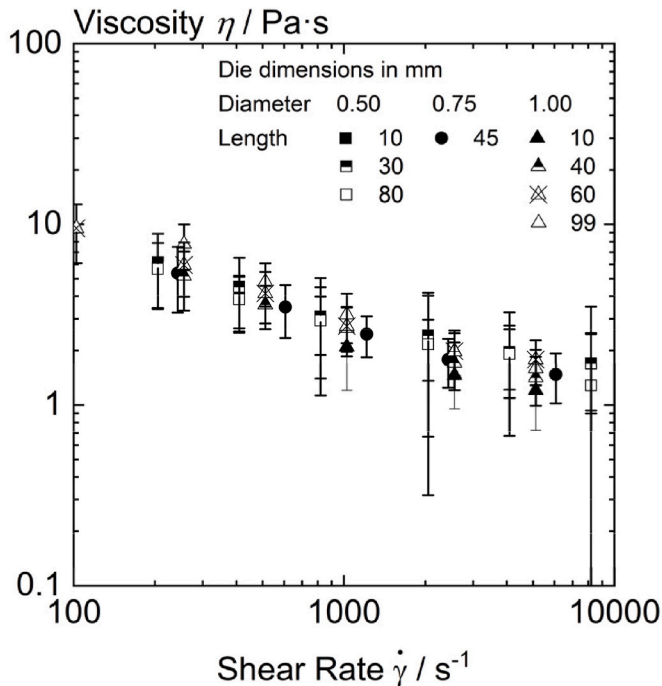


Fig. 6. Bagley corrected viscosity vs. shear rate for a paste including Texanol as bulk phase and SL1 as secondary liquid with a ratio of secondary liquid to particle volume fraction $\phi_{\text{sec}}/\phi_{\text{particle}} = 0.1$ and particle volume fraction $\phi_{\text{particle}} = 0.48$. The measurements were conducted using eight dies with different ratio of length to diameter.

3.2. Screen printing behavior of various paste compositions

Based on the results presented above regarding the slip and flow behavior of capillary suspension type model pastes, samples were selected for screen printing trials that allow to establish correlations between individual paste properties and printing results.

3.2.1. Particle volume fraction variation of yield stress and viscosity

As shown in section 3.1.1, an increase in the particle volume fraction leads to a rise in slip and yield stress, whereas the slip velocity remains constant. Since neither the primary nor the secondary phase is altered in this variation, each sample exhibits the same liquid phase viscosity and wetting properties. Furthermore, the ratio of secondary liquid to particle volume fraction $\phi_{\text{sec}}/\phi_{\text{particle}} = 0.1$ is kept constant and it can be assumed that the samples in this series exhibit similar network structure characteristics.

Table 3 summarizes the results of the screen-printing experiments obtained for this group of pastes. The particle volume fraction ϕ_{particle} of the pastes is given and from this, as well as from the viscosity of the bulk liquid η_{bulk} , the high shear viscosity η_{hs} of the pastes was estimated using the semi-empirical Maron-Pierce equation,

$$\eta_{\text{hs}} = \eta_{\text{bulk}} \left(1 - \frac{\phi_{\text{particle}}}{\phi_{\text{max}}} \right)^{-2} \quad (2)$$

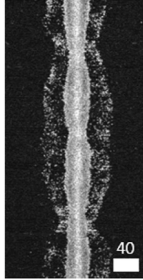
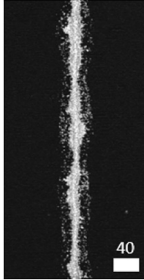
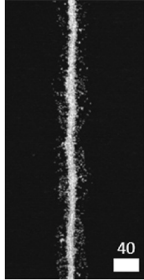
with $\phi_{\text{max}} = 0.636$ [43], valid for non-Brownian hard-sphere suspensions. The spreading of the paste between substrate and mesh and its subsequent retraction during mesh snap-off are the key process steps in fine-line screen printing. The maximum spreading width w_{max} was determined from the wetted areas adjacent to the printed line visible in the microscopy images, where individual particles remain in the pyramid structure of the substrate. The resulting line width w and height h were determined directly after printing. The cross-sectional area A corresponding to the paste laydown is calculated as $A = w \times h$.

Note, the large standard deviations provided for the line parameters (Table 3) reflects the non-uniform line shape and strong scatter in line width and height when printing the model pastes with a standard 22.5° angled screen. Nevertheless, line interruptions, i.e. cross sections with no detectable silver laydown, which would drastically reduce the cell efficiency, were not observed in any of the printing trials in this series. These deviations of the line morphology are caused by the wire crossings (so called knots) positioned in the line opening, which locally reduce the transfer of paste [51,52]. This reduction in the cross-sectional area of the line would lead to localized resistive losses. However, the printing experiment with the optimized paste using a knotless screen, maximizing open line area, in section 3.3, which also includes the electrical data, does not show these high deviations.

It is evident that a variation in the particle volume fraction, while maintaining constant slip velocity (s. Fig. 3c) and consistent wetting properties of the primary and secondary liquids, has a significant impact on the resulting spreading during the printing process and also on the final line width and height. This suggests that the latter two parameters are not decisive for the print quality in terms of achieving narrow lines and reduced laydown in frontside metallization. The rheological parameters varying with particle volume fraction are the slip stress and yield stress, as well as the high shear viscosity. The screen-printing process is a dynamic process in which the paste is constantly flowing. This is visually evident in the flooding process and by the presence of a so-called paste roll in front of the squeegee during the printing process. Nevertheless, the yield stress itself is a critical quantity, if the value is too high, no flow can be induced by the squeegee movement and thus no paste roll is formed. In this case the paste is merely pushed over the screen, which leads to process failure. On the other hand, the yield stress should not be too low to prevent gravity-driven flow of the paste through the screen openings in the flooded state. Neither of these issues occurred in any of the experiments discussed here, indicating that a yield stress

Table 3

Results of the screen-printing experiments for capillary suspension type pastes with different particle volume fractions. Texanol is used as bulk liquid and the secondary liquid is SL1. The volume fraction ratio of secondary liquid to particles is $\phi_{\text{sec}}/\phi_{\text{particle}} = 0.1$. Printing was carried out at a speed of 300 mm/s, a snap-off distance of 1 mm and a squeegee pressure of 1.5 bar. The nominal line width is 20 μm . Shown are the high shear viscosity η_{hs} estimated based on the semi-empirical Maron-Pierce equation, the maximum spreading width w_{max} , the final line width w and height h , as determined from microscopic images. The cross-sectional area is calculated as $A = w \times h$. The presence of interruptions is marked and representative sections of the lines are shown in the images.

	Particle volume fraction ϕ_{particle}		
	0.48	0.53	0.54
High shear viscosity $\eta_{\text{hs}}/\text{Pa}\cdot\text{s}$	0.22	0.47	0.57
Max. spreading width during printing $w_{\text{max}}/\mu\text{m}$	92.3 ± 26.0	39.9 ± 13.9	30.0 ± 11.4
Line width $w/\mu\text{m}$	38.9 ± 11.0	20.3 ± 7.2	16.1 ± 4.7
Line height $h/\mu\text{m}$	15.4 ± 3.9	6.9 ± 1.9	5.8 ± 1.3
Cross-sectional area $A = w \times h/\mu\text{m}^2$	599 ± 321	140 ± 88	93 ± 48
Interruptions	No	No	No
Representative section of printed lines			

range between 50 Pa and 600 Pa is suitable for fine line printing with nominal line opening widths of 20 μm . The shear stresses σ imposed on the paste during printing should be above the yield stress σ_y so that a paste roll that fills the screen can form. For the pastes investigated here, the slip stress σ_s was always below σ_y . If hypothetically, $\sigma_s < \sigma < \sigma_y$ would hold the paste would move on a slip layer over the screen, but there would be no flow and thus no paste roll. A similar phenomenon would appear in a flow regime, where slip and flow coexist, but slip dominates. This was not observed in the printing trials conducted for this paste group. So, we conclude, that the quantity mainly determining line width and laydown is the high shear viscosity. Our data suggest that $w \sim 1/\eta_{\text{hs}}$ as shown in Fig. 7.

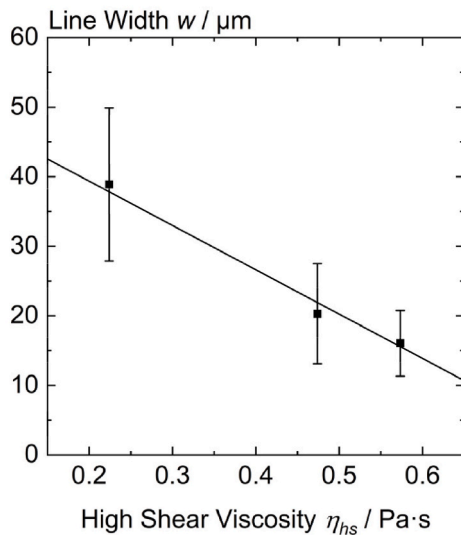


Fig. 7. Final line width w from the screen-printing experiments of pastes with the particle volume fractions 0.48, 0.53 and 0.54 (dots from left to right) in Texanol with secondary liquid SL1, added in the ratio $\phi_{\text{sec}}/\phi_{\text{particle}} = 0.1$. The width is plotted against the estimated high shear viscosity obtained by using the semi-empirical Maron-Pierce equation. Printing was performed at a speed of 300 mm/s, a snap-off distance of 1 mm and a squeegee pressure of 1.5 bar. The nominal line width is 20 μm . The solid line marks a linear fit to the experimental data yielding a regression coefficient $R^2 = 0.98$.

This is in line with earlier results for ZnO pastes including polymeric rheology control agents [46]. In this study it was, however, observed, that the yield stress has an effect on the length of the pre-injection zone and thus on paste transfer and line width. Accordingly, a scaling law $w \sim 1/(\eta_{\text{hs}} \times \sigma_y)$ was suggested in this work, but for the data obtained here the regression coefficient is slightly lower using this scaling than for the simple $w \sim 1/\eta_{\text{hs}}$ correlation. The role of the yield stress will be discussed in more detail in the next section.

3.2.2. Effect of secondary liquid content – variation of slip and yield stress

A direct comparison between the printing behavior of a suspension with and without secondary liquid phase has been performed. The particle volume fraction as well as the bulk liquid and thus the high shear viscosity and wetting of both suspensions are equal. However, the capillary suspension exhibits a much higher network strength than the binary suspension, showing up in an almost tenfold higher yield stress (Fig. 4). Accordingly, printing trials on these samples allow for a separation of viscosity and yield stress contributions and will inform us about the effect of the latter on the finger line properties. Test results are summarized in Table 4, including the spreading width during the printing process w_{max} , the final line width w , the final line height h as well as the cross-sectional area $A = w \times h$.

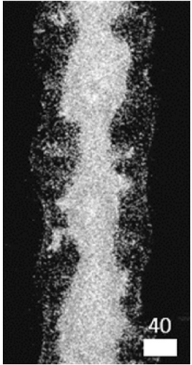
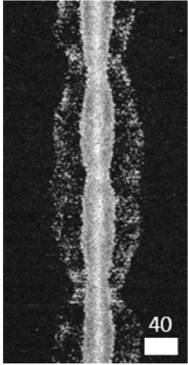
Obviously, the higher yield stress of the capillary suspension results in narrower but higher printed lines. The cross-sectional area, however, is the same within experimental uncertainty. The sample with a higher yield stress exhibits less spreading and stronger retraction. The former is attributed to the higher yield stress, which means that a larger part of the applied pressure is required to break the strong network structure. The latter may be due to stronger slip (Fig. 4) and rapid structural recovery typically found in capillary suspensions [42] stabilizing a high aspect ratio h/w .

Based on the results presented in sections 3.1.2 and 3.2.2 we conclude, that the high shear viscosity is the key parameter controlling paste transfer and final line width. A high paste viscosity is mandatory to reduce paste consumption.

In 3.1.2, it was shown that capillary suspensions with $\phi_{\text{sec}}/\phi_{\text{particle}} \geq 0.1$ exhibit a plateau in slip and yield stress, but show an essentially linear increase in slip velocity with increasing $\phi_{\text{sec}}/\phi_{\text{particle}}$ (Fig. 4). This enables us to assess the effect of this paste property on printing behavior while keeping slip and yield stress, as well as viscosity and wetting

Table 4

Results of the screen-printing experiments for pastes with and without secondary liquid addition. The particle volume fraction is $\phi_{particle} = 0.48$. Texanol is used as bulk liquid and the secondary liquid is SL1. Printing was carried out at a speed of 300 mm/s, a snap-off distance of 1 mm and a squeegee pressure of 1.5 bar. The nominal line width is 20 μm . Shown are the maximum spreading width w_{max} , the final line width w and height h , as determined from microscopic images. The cross-sectional area is calculated as $A = w \times h$. The presence of interruptions is marked and representative sections of the lines are shown in the images.

	$\phi_{sec} / \phi_{particle}$	
	0	0.1
Maximum spreading width during printing $w_{max}/\mu\text{m}$	125.4 ± 24.7	92.3 ± 26.0
Line width $w/\mu\text{m}$	66.7 ± 17.9	38.9 ± 11.0
Line height $h/\mu\text{m}$	9.3 ± 2.9	15.4 ± 3.9
Cross-sectional area $A = w \times h/\mu\text{m}^2$	620 ± 360	599 ± 321
Interruptions	No	No
Representative section of printed lines		

properties constant. The results of printing trials for three selected pastes from this group are summarized in Table 5.

As shown in Table 6, it is evident that increasing the slip velocity, results in reduced spreading during the printing process as well as lower final line widths and line heights. With a slip velocity of 4.3 ± 0.1 mm/s the paste transfer is strongly reduced compared to the paste with a slip velocity of 3.6 ± 0.3 mm/s and the printed finger lines are very inhomogeneous. The paste transfer decreases further with increasing slip

Table 5

Results of the screen-printing experiments for pastes with varying ratios of secondary liquid to particle volume fraction $\phi_{sec} / \phi_{particle}$. The particle volume fraction is 0.48. Texanol is used as bulk liquid and the secondary liquid is SL1. The printing was carried out at a speed of 300 mm/s, a snap-off distance of 1 mm and a squeegee pressure of 1.5 bar. The nominal line width is 20 μm . Shown are the maximum spreading width w_{max} , the final line width w and height h , as determined from microscopic images. The cross-sectional area is calculated as $A = w \times h$. The presence of interruptions is marked and representative sections of the lines are shown in the images.

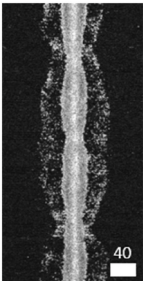
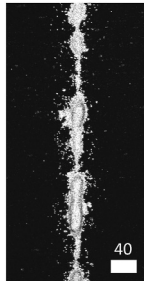
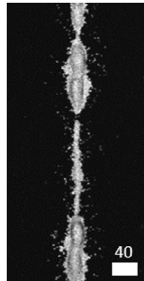
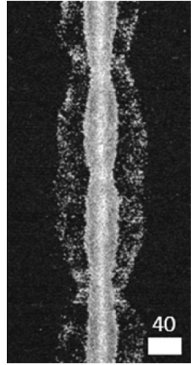
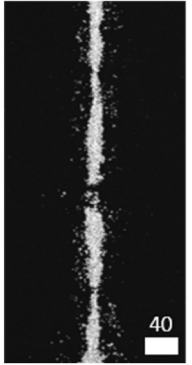
	$\phi_{sec} / \phi_{particle}$		
	0.1	0.19	0.26
Slip velocity $v_s/\text{mm}\cdot\text{s}^{-1}$	3.6 ± 0.3	4.3 ± 0.1	5.3 ± 0.2
Maximum spreading width during printing $w_{max}/\mu\text{m}$	92.3 ± 26.0	33.1 ± 18.1	31.0 ± 16.7
Line width $w/\mu\text{m}$	38.9 ± 11.0	19.7 ± 8.9	18.7 ± 9.5
Line height $h/\mu\text{m}$	15.4 ± 3.9	10.2 ± 6.2	9.6 ± 6.6
Cross-sectional area $A = w \times h/\mu\text{m}^2$	599 ± 321	201 ± 213	180 ± 215
Interruptions	No	No	Yes
Representative section of printed lines			

Table 6

Results of the screen-printing experiments of pastes with different types of secondary liquid. The particle volume fraction is 0.48. The bulk liquid is Texanol. The secondary liquids vary in their interfacial tension Γ and also result in varying paste yield stresses σ_y as well as slip velocities v_s at 290 Pa. The printing was carried out at a speed of 300 mm/s, a snap-off distance of 1 mm and a squeegee pressure of 1.5 bar. The nominal line width is 20 μm . Shown are the maximum spreading width w_{max} , the final line width w and height h , as determined from microscopic images. The cross-sectional area is calculated as $A = w \times h$. The presence of interruptions is marked and representative sections of the lines are shown in the images.

	Type of secondary liquid	
	SL1 ($\Gamma = 0.2$ mN/m, $\sigma_y = 410$ Pa, $v_s = 3.6$ mm/s)	SL3 ($\Gamma = 0.5$ mN/m, $\sigma_y = 520$ Pa, $v_s = 5.3$ mm/s)
Maximum spreading width during printing $w_{max}/\mu\text{m}$	92.3 ± 26.0	27.1 ± 14.9
Line width $w/\mu\text{m}$	38.9 ± 11.0	14.3 ± 6.1
Line height $h/\mu\text{m}$	15.4 ± 3.9	4.8 ± 1.7
Cross-sectional area $A = w \times h/\mu\text{m}^2$	599 ± 321	69 ± 54
Interruptions	No	Yes
Representative section of printed lines		

velocity. Many areas can be seen where almost no paste was transferred and a large number of line interruptions was detected. While narrower lines and a lower paste transfer are generally desirable for metallization fingers, the strong inhomogeneities, which are reflected in the large standard deviation for w or h and can be clearly seen in the

representative sections of the printed lines (Table 5), make these pastes unsuitable for fine-line printing. The reason for this is that slip already occurs above the screen, which affects the paste roll and flooding behavior during printing. For pastes with high slip the paste roll does not form properly, and the paste is merely pushed over the screen during printing and flooding. This prevents uniform filling of the screen openings and results in the depicted inhomogeneous paste transfer with strong variations in height. To characterize this in more detail, Fig. 8 compares the distribution of measured heights along the printed lines for the pastes with $\phi_{\text{sec}}/\phi_{\text{particle}} = 0.1$ and 0.26.

The paste with $\phi_{\text{sec}}/\phi_{\text{particle}} = 0.1$ predominantly shows height variations above the emulsion over mesh (EOM) height and exhibits only few regions showing line heights below the EOM thickness. In contrast, for the paste with $\phi_{\text{sec}}/\phi_{\text{particle}} = 0.26$ and high slip velocity the majority of measured line heights is below the EOM. Additionally, a small number of very high line heights is observed. The distribution is broad and bimodal, whereas the sample with less slip exhibits a narrower monomodal line height distribution. Especially, the regions of line heights below EOM corresponding to incomplete filling are supposed to be detrimental to electrical conductivity or cell performance and must be avoided. Previously, it was shown [20] that stronger paste slip promotes mesh emptying and increases paste laydown. In this study, pastes showed similar yield stress as the series of pastes investigated here, the slip velocity, however, was about 5 times lower and slip on the screen surface did not occur. The benefit of slip for mesh emptying was also confirmed in another study [31] employing screens with different surface treatment and showing that paste transfer was higher, when the adhesion of the paste to the screen was reduced.

Placing this finding within previous investigations enables the definition of a slip velocity range in which slip can lead to an improvement in print result. For pastes with slip velocity values between 0.005 and 0.050 mm/s no effect of slip on paste transfer was observed in corresponding printing experiments [24]. Increasing slip velocity from 0.25 to 1.25 mm/s at a shear stress of 300 Pa significantly enhanced paste transfer and line height [30]. The experimental data presented here show that process failure and line inhomogeneities begin to occur when the slip velocity increases from 3.6 to 4.3 mm/s, and further increase at a slip velocity of 5.3 mm/s. Based on these studies, the optimal slip velocity range can be narrowed down to $0.25 < v_s < 3.6$ mm/s at 290 ± 10 Pa as process failure due to slip above the screen occurs between 3.6 and 4.3 mm/s and further increases at a slip velocity of 5.3 mm/s at a shear stress of 290 Pa, and no influence of slip was found for slip velocities about an order of magnitude below 0.25 mm/s.

3.2.3. Type of secondary liquid

It remains to be clarified whether only the slip velocity of the paste or also the type of secondary liquid is responsible for the phenomena described in 3.2.2. Pastes were prepared with secondary liquid SL1 and SL3, with $\phi_{\text{sec}}/\phi_{\text{particle}} = 0.1$ in both cases. Due to their different interfacial tension with Texanol (s. 3.1.3) these fluids provide pastes with different yield stress, slip velocity is also different, but the slip stress is essentially the same (Fig. 5). Since these pastes include the same bulk liquid and particle loading their high shear viscosity and wetting properties are also similar.

Consistent with the results discussed above paste transfer is significantly reduced for the sample with the higher slip velocity of 5.3 ± 0.4 mm/s, and line inhomogeneities with many interruptions are observed. This suggests that not the type of secondary liquid, but the prevailing slip velocity of the paste is relevant. Once again, slip on the screen surface causes poor paste rolling and flooding for the paste with high slip velocity (SL3), and hence insufficient paste transfer. Fig. 9a shows a histogram of measured line heights, essentially all line heights are below emulsion over mesh (EOM) clearly confirming incomplete paste transfer. Fig. 9b depicts a photo of the poor flooding due to excessive slip. As can be seen, the paste was merely pushed over the screen by the flooding squeegee, but no flow of the paste occurred, and after a short distance an almost clean instead of a flooded screen remains. This occurs analogously in front of the printing squeegee, so that a paste roll cannot form.

Overall, our results demonstrate that excessively high slip velocities lead to process failure above the screen and cannot contribute to improving the printed line quality. It should be noted, that the observations made here using different secondary liquids but the same bulk fluid are consistent with the previous assumption (s. 3.2.3) that the bulk liquid, and not the secondary liquid, is located in the slip layer.

3.3. Formulation of a high-temperature metallization paste product

The findings described above were applied in the formulation of a proprietary high-temperature metallization paste system.

Fig. 10 shows the adjustment of the desired line width by a targeted increase in viscosity for a sample series including pastes with different silver content and vehicle viscosity. The yield stress varies in the same range as for the pastes discussed above, but the slip velocity was an order of magnitude lower. The line width was obtained in printing trials using a knotless screen with 12 μm nominal line width. These data confirm the relationship $w \sim 1/\eta_{\text{hs}}$ already shown in Fig. 6.

For the paste with the lowest achieved average line width, the line morphology in the printing experiment (a), the distribution of line heights (b), as well as an exemplary 3D image and top views with and without topography (c) and the electrical data achieved in the

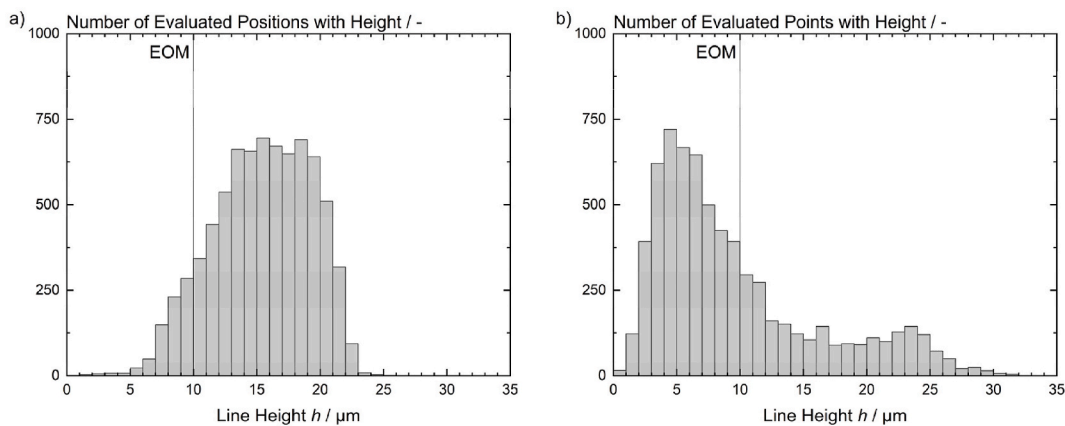


Fig. 8. Evaluation of the heights from nine randomly distributed microscope images per group for pastes including 48 vol% particles in Texanol and $\phi_{\text{sec}}/\phi_{\text{particle}} = 0.1$ (a) or 0.26 (b). The secondary liquid SL1 is used for both pastes. Each pixel row in the laser microscopic images was analyzed and classified to obtain the histograms. The vertical line indicates the emulsion over mesh height of 10 μm .

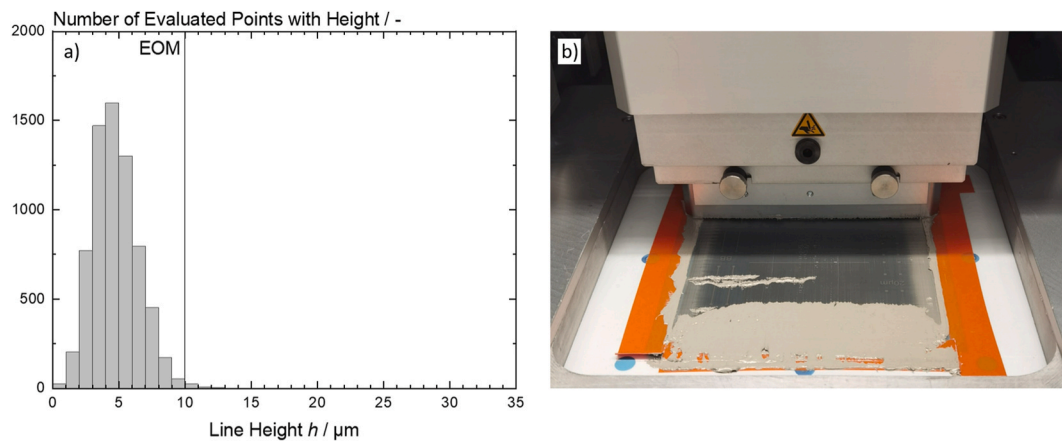


Fig. 9. a) Evaluation of the heights from nine randomly distributed microscope images of the paste including 48 vol% particles in Texanol and $\phi_{\text{sec}} / \phi_{\text{particle}} = 0.1$. The secondary liquid is SL3. Each pixel row in the laser microscopic images was analyzed and classified to obtain the histogram. The vertical line indicates the emulsion over mesh (EOM) height of 10 μm . b) Photography of the screen after the flooding process in a printing cycle. Failures in the correct flooding of the screen due to excessive slip are clearly visible by the paste-free area revealing the bare screen emulsion instead of a paste covered surface.

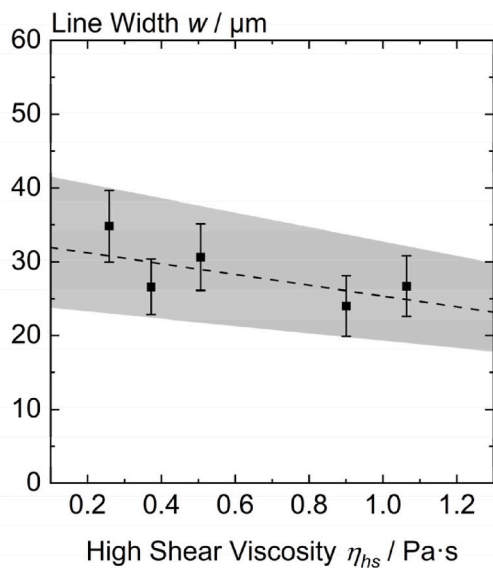


Fig. 10. Obtained line width in the printing experiment in relation to the high shear viscosity. Shown pastes with varying particle content and vehicle composition. The dashed linear depicts a linear fit. The grey area indicates the general trend with respect to the measured standard deviations. Printing was done on a knotless screen with 12 μm nominal line width and 10 μm emulsion over mesh (EOM) at 500 mm/s speed, 1 mm snap-off distance and 2 bar pressure.

metallization of PERC cells with the help of a project partner (d) are shown in Fig. 11.

Using this paste a printed line width of $24 \pm 4.1 \mu\text{m}$ and an aspect ratio $h/w = 0.48 \pm 0.12$ was obtained, with the measured heights lying in a narrow range above the EOM height apart from a few typical screen-printing mesh marks. In the metallization of PERC cells with the help of a project partner, efficiencies of 23.53 ± 0.06 were achieved on an industry-standard setup.

This example demonstrates that based on the correlations outlined above high-quality metallization pastes for fine line screen printing can be formulated.

4. Conclusion

The present study investigates how rheological properties of metal-

lization pastes, including yield stress and high shear viscosity as well as slip stress and slip velocity, affect the results of fine-line screen printing. The study focuses on spreading width, final line width and height, as well as line uniformity and interruptions. A model system based on the principle of capillary suspensions was designed allowing for selective and systematic variation of these properties in a simple manner. Silver pastes using Texanol as the bulk liquid and four secondary liquids showing different interfacial tension with Texanol were employed. These capillary suspensions exhibit pronounced wall slip at stresses below the yield stress σ_y , which sets in at a critical stress termed slip stress $\sigma_s < \sigma_y$, and it was confirmed that the bulk liquid, not the secondary liquid, is present in the slip layer.

Firstly, the particle volume fraction ϕ_{particle} is varied while maintaining the ratio of secondary liquid to particle volume fraction constant. In this series the paste viscosity varies with ϕ_{particle} according to Eq. (2), and additionally, the yield stress as well as the slip stress increase with increasing particle fraction, whereas the slip velocity remained constant around 3.5 mm/s. The corresponding printing experiments demonstrated that an increase in paste viscosity and yield stress, resulted in less pronounced spreading, narrower final line width, and reduced paste laydown. In the second part of the study, the ratio of the secondary liquid to particle volume fraction is increased while keeping the particle volume fraction constant. This keeps the high shear viscosity of the paste constant, whereas the yield stress strongly increases, finally reaching a plateau, as expected for capillary suspensions, and the slip stress also follows a similar trend. The slip velocity, however, does not plateau but increases linearly from 2.8 to 5.4 mm/s. Printing trials on these samples allowed for a separation of viscosity and yield stress contributions. The capillary suspension with a higher yield stress exhibits less spreading and stronger retraction, but the same cross-sectional area, i.e. a similar paste laydown.

From these results we conclude that high shear viscosity is the key parameter controlling paste transfer and final line width. A high paste viscosity is essential to achieve a narrow line width and reduced paste consumption.

When comparing three pastes with increasing secondary liquid fractions, it is observed that a significant increase in slip velocity from 3.6 to 5.4 mm/s causes inhomogeneities in line morphology. In addition, paste transfer is reduced. This phenomenon can be attributed to excessive slip above the screen, which hinders paste roll formation and screen filling. This complements previous studies which reported that increased paste slip promotes mesh emptying and increases paste deposition at slip velocities starting at 0.25 mm/s [30,31], but no effect of slip velocity on paste transfer was found at velocities in the range between 0.005 and

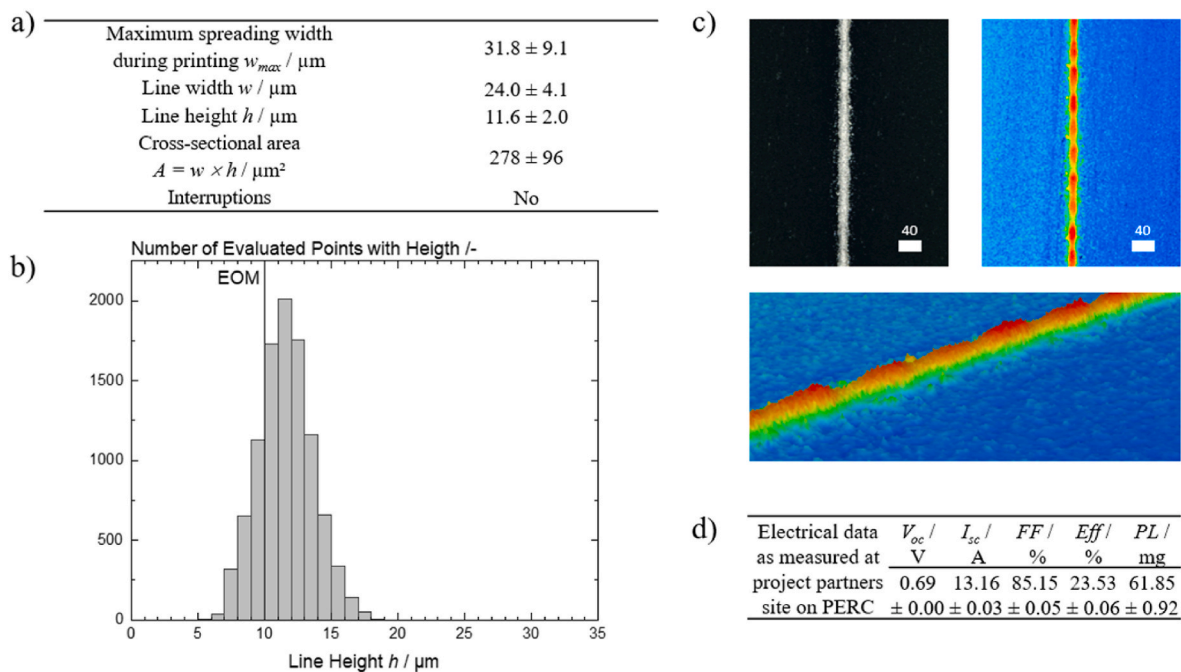


Fig. 11. a) Results of the screen-printing experiments at a speed of 500 mm/s, a snap-off distance of 1 mm and a squeegee pressure of 2 bar. The nominal line width is 12 μm on a knotless screen with an emulsion over mesh (EOM) thickness of 10 μm . Shown are the maximum spreading width w_{max} , the final line width w and height h , as determined from microscopic images. The cross-sectional area is calculated as $A = w \times h$. The presence of interruptions is marked. b) Evaluation of the heights from nine randomly distributed microscope images of these printing experiments. Each pixel row in the laser microscopic images was analyzed and classified to obtain the histogram. The vertical line indicates the EOM height of 10 μm . c) Top view of representative section of printed lines with and without topography as well as 3D image, as derived from laser microscopy d) The paste was used in the R&D center of a project partner to metallize PERC cells and the resulting electrical data (open circuit voltage V_{oc} , short circuit current I_{sc} , fill factor FF , and efficiency Eff) as well as the paste laydown PL are shown.

0.05 mm/s [24]. Based on this, we conclude that there is an optimum slip range in which slip can lead to an improvement in the print result between 0.25 and 3.6 mm/s at 290 ± 10 Pa, as process failure due to slip above the screen starts to occur between 3.6 and 4.3 mm/s, and no influence of slip was found for slip velocities about an order of magnitude below 0.25 mm/s [24]. This result is further supported by comparing the printing results of two pastes containing different secondary liquids. The secondary liquid with the higher interfacial tension to the bulk liquid not only increases the yield stress, as expected, but also increases the slip velocity from 3.6 to 5.3 mm/s, again resulting in an inhomogeneous line morphology due to insufficient paste transfer.

We have used these findings to develop a ready-to-use metallization paste yielding a line width of 24 μm and an aspect ratio of 0.48 when printed through at 12 μm knotless screen, and achieved a cell efficiency of 23.53 % on PERC cells, with a laydown that was 16 % lower compared to commercial reference pastes [2].

Here we have investigated the screen-printing behavior of pastes containing a Newtonian bulk fluid, highlighting the effects of paste yield stress, viscosity and slip on printing results. This will support the future development of metallization pastes to help reduce silver consumption in the PV industry. However, commercial pastes typically contain high molecular weight polymers as rheology modifiers, which may imply a viscoelastic response during processing; the influence of this rheological property should be the subject of future work.

CRedit authorship contribution statement

Max Ailinger: Writing – review & editing, Writing – original draft, Visualization, Validation, Supervision, Software, Resources, Project administration, Methodology, Investigation, Funding acquisition, Formal analysis, Data curation, Conceptualization. **Karim Abdel Aal:** Writing – review & editing, Writing – original draft, Visualization, Validation, Supervision, Software, Resources, Project administration,

Methodology, Investigation, Funding acquisition, Formal analysis, Data curation, Conceptualization. **Norbert Willenbacher:** Writing – review & editing, Writing – original draft, Visualization, Validation, Supervision, Software, Resources, Project administration, Methodology, Investigation, Funding acquisition, Formal analysis, Data curation, Conceptualization.

Declaration of generative AI and AI-assisted technologies in the writing process

During the preparation of this work the authors used DeepL and Microsoft Copilot in order to improve the readability and language. After using this tool/service, the authors reviewed and edited the content as needed and take full responsibility for the content of the published article.

Declaration of competing interest

The authors declare the following financial interests/personal relationships which may be considered as potential competing interests: Norbert Willenbacher has patent #EP 3 446 337 B1 issued to Karlsruhe Institute of Technology (KIT). If there are other authors, they declare that they have no known competing financial interests or personal relationships that could have appeared to influence the work reported in this paper.

Acknowledgements

We highly acknowledge the financial support of the Karlsruhe Institute of Technology (Strategiefonds) and the support of our student assistants Aurelia Kuhn, Dilara Örtel, and Maren Gehrlein for their help with the measurement work for this publication.

Data availability

All data except the parts marked as proprietary will be made available on request.

References

- [1] D. Feldman, J. Zuboy, K. Dummit, D. Stright, M. Heine, S. Grossman, Stright Matthew, R. Margolis, Summer 2024: Solar Industry Update, 2024.
- [2] M. Fischer, M. Woodhouse, P. Baliozian, International Technology Roadmap for Photovoltaics (ITRPV) 2023 Results, fifteenth ed., 2024.
- [3] Silver Supply and Demand | The Silver Institute, The Silver Institute (n.d.). https://silverinstitute.org/silver-supply-demand/#silver_demand (accessed March 11, 2025).
- [4] N.A. Latif, D. von Kutzleben, J. Weber, T. Röbler, J. Markert, J.D. Huyeng, E. Lohmüller, S. Birnkammer, L.E. Alanis, A. Kraft, H. Neuhaus, Advancements in shingle matrix technology for high volume production, in: 2024 IEEE 52nd Photovoltaic Specialist Conference (PVSC), IEEE, 2024, pp. 605–611, <https://doi.org/10.1109/PVSC57443.2024.10748959>.
- [5] Y. Zhang, M. Kim, L. Wang, P. Verlinden, B. Hallam, Design considerations for multi-terawatt scale manufacturing of existing and future photovoltaic technologies: challenges and opportunities related to silver, indium and bismuth consumption, Energy Environ. Sci. 14 (2021) 5587–5610, <https://doi.org/10.1039/D1EE01814K>.
- [6] E. Hornbogen, H. Warlimont, B. Skrotzki, Metalle, Springer Vieweg, Berlin, 2019, <https://doi.org/10.1007/978-3-662-57763-9>.
- [7] J. Lindroos, H. Savin, Review of light-induced degradation in crystalline silicon solar cells, Sol. Energy Mater. Sol. Cell. 147 (2016) 115–126, <https://doi.org/10.1016/j.solmat.2015.11.047>.
- [8] R. Lago, L. Pérez, H. Kerp, I. Freire, I. Hoces, N. Azkona, F. Recart, J.C. Jimeno, Screen printing metallization of boron emitters, Prog. Photovoltaics Res. Appl. 18 (2010) 20–27, <https://doi.org/10.1002/ppp.933>.
- [9] M. Ju, Y.-J. Lee, J. Lee, B. Kim, K. Ryu, K. Choi, K. Song, K. Lee, C. Han, Y. Jo, J. Yi, Double screen printed metallization of crystalline silicon solar cells as low as 30µm metal line width for mass production, Sol. Energy Mater. Sol. Cell. 100 (2012) 204–208, <https://doi.org/10.1016/j.solmat.2012.01.018>.
- [10] V. Shanmugam, J. Wong, I.M. Peters, J. Cunnusamy, M. Zahn, A. Zhou, R. Yang, X. Chen, A.G. Aberle, T. Mueller, Analysis of fine-line screen and stencil-printed metal contacts for silicon wafer solar cells, IEEE J. Photovoltaics 5 (2015) 525–533, <https://doi.org/10.1109/JPHOTOV.2014.2388073>.
- [11] A.W. Blakers, Shading losses of solar-cell metal grids, J. Appl. Phys. 71 (1992) 5237–5241, <https://doi.org/10.1063/1.350580>.
- [12] L. Wang, C. Guo, R.M. Cosimano, W. Zhang, Conductive Thick Film Paste for Solar Cell Contacts, 2015. US 8,952,245 B2.
- [13] S.J. Jeon, S.M. Koo, S.A. Hwang, Optimization of lead- and cadmium-free front contact silver paste formulation to achieve high fill factors for industrial screen-printed Si solar cells, Sol. Energy Mater. Sol. Cell. 93 (2009) 1103–1109, <https://doi.org/10.1016/j.solmat.2009.01.003>.
- [14] G. Laudisio, R. Young, James Peter, K. Hang, Metal Pastes and Use Thereof in the Production of Silicon Solar Cells, 2010. US 2010/0243048 A1.
- [15] K.W. Hang, G. Laudisio, Y. Wang, R.S. Watt, Conductive metal paste and use thereof, US 2013/0192671 A1 (2013).
- [16] C. Yüce, K. Okamoto, L. Karpowich, A. Adrian, N. Willenbacher, Non-volatile free silver paste formulation for front-side metallization of silicon solar cells, Sol. Energy Mater. Sol. Cell. 200 (2019) 110040, <https://doi.org/10.1016/j.solmat.2019.110040>.
- [17] J. Hoorstra, A.W. Weeber, H.H.C. De Moor, W.C. Sinke, The importance of paste rheology in improving fine line. Thick Film Screen Printing of Front Side Metallization, Netherlands Energy Research Foundation ECN, 1997.
- [18] M. Pospischil, J. Specht, M. König, M. Hörter, C. Mohr, F. Clement, D. Biro, Paste rheology correlating with dispensed finger geometry, IEEE J. Photovoltaics 4 (2014) 498–503, <https://doi.org/10.1109/JPHOTOV.2013.2278657>.
- [19] S. Thibert, J. Jourdan, B. Bechevet, D. Chaussy, N. Reverdy-Bruas, D. Beneventi, Influence of silver paste rheology and screen parameters on the front side metallization of silicon solar cell, Mater. Sci. Semicond. Process. 27 (2014) 790–799, <https://doi.org/10.1016/j.mssp.2014.08.023>.
- [20] C. Xu, N. Willenbacher, How rheological properties affect fine-line screen printing of pastes: a combined rheological and high-speed video imaging study, J. Coating Technol. Res. 15 (2018) 1401–1412, <https://doi.org/10.1007/s11998-018-0091-2>.
- [21] C.P. Hsu, R.H. Guo, C.C. Hua, C.L. Shih, W.T. Chen, T.I. Chang, Effect of polymer binders in screen printing technique of silver pastes, J. Polym. Res. 20 (2013) 1–8, <https://doi.org/10.1007/s10965-013-0277-3>.
- [22] R. Faddoul, N. Reverdy-Bruas, J. Bourel, Silver content effect on rheological and electrical properties of silver pastes, J. Mater. Sci. Mater. Electron. 23 (2012) 1415–1426, <https://doi.org/10.1007/s10854-011-0607-3>.
- [23] S. Tepner, N. Wengenmeyr, M. Linse, A. Lorenz, M. Pospischil, F. Clement, The link between Ag-paste rheology and screen-printed solar cell metallization, Adv. Mater. Technol. 5 (2020) 1–9, <https://doi.org/10.1002/admt.202000654>.
- [24] C. Yüce, M. König, N. Willenbacher, Rheology and screen-printing performance of model silver pastes for metallization of Si-solar cells, Coatings (Oakv.) 8 (2018) 406, <https://doi.org/10.3390/coatings8110406>.
- [25] H.A. Barnes, A review of the slip (wall depletion) of polymer solutions, emulsions and particle suspensions in viscometers: its cause, character, and cure, J. Nonnewton Fluid Mech. 56 (1995) 221–251, [https://doi.org/10.1016/0377-0257\(94\)01282-M](https://doi.org/10.1016/0377-0257(94)01282-M).
- [26] M. Cloitre, R.T. Bonnecaze, A review on wall slip in high solid dispersions, Rheol. Acta 56 (2017) 283–305, <https://doi.org/10.1007/s00397-017-1002-7>.
- [27] D.M. Kalyon, S. Aktaş, Factors affecting the rheology and processability of highly filled suspensions, Annu. Rev. Chem. Biomol. Eng. 5 (2014) 229–254, <https://doi.org/10.1146/annurev-chembioeng-060713-040211>.
- [28] U. Yilmazer, D.M. Kalyon, Slip effects in capillary and parallel disk torsional flows of highly filled suspensions, J. Rheol. 33 (1989) 1197–1212, <https://doi.org/10.1122/1.550049>.
- [29] D.M. Kalyon, Apparent slip and viscoplasticity of concentrated suspensions, J. Rheol. 49 (2005) 621–640, <https://doi.org/10.1122/1.1879043>.
- [30] C. Xu, M. Fies, N. Willenbacher, Impact of wall slip on screen printing of front-side silver pastes for silicon solar cells, IEEE J. Photovoltaics 7 (2017) 129–135, <https://doi.org/10.1109/JPHOTOV.2016.2626147>.
- [31] S. Tepner, N. Wengenmeyr, L. Ney, M. Linse, M. Pospischil, F. Clement, Improving wall slip behavior of silver pastes on screen emulsions for fine line screen printing, Sol. Energy Mater. Sol. Cell. 200 (2019) 109969, <https://doi.org/10.1016/j.solmat.2019.109969>.
- [32] F. Soltani, Ü. Yilmazer, Slip velocity and slip layer thickness in flow of concentrated suspensions, J. Appl. Polym. Sci. 70 (1998) 515–522, [https://doi.org/10.1002/\(SICI\)1097-4628\(19981017\)70:3<515::AID-APP13>3.0.CO;2-6%23](https://doi.org/10.1002/(SICI)1097-4628(19981017)70:3<515::AID-APP13>3.0.CO;2-6%23).
- [33] S.C. Jana, B. Kapoor, A. Acrivos, Apparent wall slip velocity coefficients in concentrated suspensions of noncolloidal particles, J. Rheol. 39 (1995) 1123–1132, <https://doi.org/10.1122/1.550631>.
- [34] E.C. Bingham, Fluidity and Plasticity, first ed., McGraw-Hill Book Company, Inc., New York, 1922.
- [35] M. Mooney, Explicit formulas for slip and fluidity, J. Rheol. 2 (1931) 210–222, <https://doi.org/10.1122/1.2116364>.
- [36] A. Yoshimura, R.K. Prud'homme, Wall slip corrections for Couette and parallel disk viscometers, J. Rheol. 32 (1988) 53–67, <https://doi.org/10.1122/1.549963>.
- [37] D.E. Riemer, The theoretical fundamentals of the screen printing process, Microelectron. Int. 6 (1989) 8–17, <https://doi.org/10.1108/eb044350>.
- [38] K. Abdel Aal, N. Willenbacher, Front side metallization of silicon solar cells – a high-speed video imaging analysis of the screen printing process, Sol. Energy Mater. Sol. Cell. 217 (2020) 110721, <https://doi.org/10.1016/j.solmat.2020.110721>.
- [39] E. Koos, N. Willenbacher, Capillary forces in suspension rheology, Science 331 (2011) 897–900, <https://doi.org/10.1126/science.1199243>, 1979.
- [40] E. Koos, Capillary suspensions: particle networks formed through the capillary force, Curr. Opin. Colloid Interface Sci. 19 (2014) 575–584, <https://doi.org/10.1016/j.cocis.2014.10.004>.
- [41] M. Schneider, E. Koos, N. Willenbacher, Highly conductive, printable pastes from capillary suspensions, Sci. Rep. 6 (1 6) (2016) 1–10, <https://doi.org/10.1038/srep31367>, 2016.
- [42] E. Koos, J. Johannsmeier, L. Schwebler, N. Willenbacher, Tuning suspension rheology using capillary forces, Soft Matter 8 (2012) 6620–6628, <https://doi.org/10.1039/C2SM25681A>.
- [43] J. Mewis, N.J. Wagner, Colloidal Suspension Rheology, Cambridge University Press, Cambridge, 2012, <https://doi.org/10.1017/CBO9780511977978>.
- [44] J. Maurath, B. Bitsch, Y. Schwegler, N. Willenbacher, Influence of particle shape on the rheological behavior of three-phase non-brownian suspensions, Colloids Surf. A Physicochem. Eng. Asp. 497 (2016) 316–326, <https://doi.org/10.1016/j.colsurfa.2016.03.006>.
- [45] C. Yüce, N. Willenbacher, Challenges in rheological characterization of highly concentrated suspensions - a case study for screen-printing silver pastes, JoVE J. (2017) 1–17, <https://doi.org/10.3791/55377>.
- [46] B.K. Aral, D.M. Kalyon, Effects of temperature and surface roughness on time-dependent development of wall slip in steady torsional flow of concentrated suspensions, J. Rheol. 38 (1994) 957–972, <https://doi.org/10.1122/1.550537>.
- [47] E.B. Bagley, The separation of elastic and viscous effects in polymer flow, Trans. Soc. Rheol. 5 (1961) 355–368, <https://doi.org/10.1122/1.548905>.
- [48] E.B. Bagley, End corrections in the capillary flow of polyethylene, J. Appl. Phys. 28 (1957) 624–627, <https://doi.org/10.1063/1.1722814>.
- [49] F. Bossler, E. Koos, Structure of particle networks in capillary suspensions with wetting and nonwetting fluids, Langmuir 32 (2016) 1489–1501, <https://doi.org/10.1021/acs.langmuir.5b04246>.
- [50] S. Hoffmann, E. Koos, N. Willenbacher, Using capillary bridges to tune stability and flow behavior of food suspensions, Food Hydrocoll. 40 (2014) 44–52, <https://doi.org/10.1016/j.foodhyd.2014.01.027>.
- [51] S. Tepner, L. Ney, M. Linse, A. Lorenz, M. Pospischil, F. Clement, Studying knotless screen patterns for fine-line screen printing of Si-solar cells, IEEE J. Photovoltaics 10 (2020) 319–325, <https://doi.org/10.1109/JPHOTOV.2019.2959939>.
- [52] T. Wenzel, A. Lorenz, E. Lohmüller, S. Auerbach, K. Masuri, Y.C. Lau, S. Tepner, F. Clement, Progress with screen printed metallization of silicon solar cells - towards 20 µm line width and 20 mg silver laydown for PERC front side contacts, Sol. Energy Mater. Sol. Cell. 244 (2022) 111804, <https://doi.org/10.1016/j.solmat.2022.111804>.